Comparison of pinning parameters between low-T_c superconductors and $YBa_2Cu_3O_{7-\delta}$

H. Küpfer
Forschungszentrum Karlsruhe, Institut für Technische Physik and Universität Karlsruhe, Postfach 3640, D-76021 Karlsruhe, Germany

A. A. Zhukov
Forschungszentrum Karlsruhe, Institut für Technische Physik, Postfach 3640, D-76027 Karlsruhe, Germany and Physics Department, Moscow State University, 117234 Moscow, Russia

R. Kresse, R. Meier-Hirmer, W. Jahn, and T. Wolf
Forschungszentrum Karlsruhe, Institut für Technische Physik and Universität Karlsruhe, Postfach 3640, D-76021 Karlsruhe, Germany

T. Matsushita
Department of Computer Science and Electronics, Kyushu Institute of Technology, 680-4 Kawazu, Iizuka 820, Japan

K. Kimura
Advanced Materials and Technology Research Laboratories, Nippon Steel Co., 1618 Ida, Nakahara-Ku, Kawasaki 211, Japan

K. Salama
Department of Mechanical Engineering, Texas Center of Superconductivity at University of Houston, Houston, Texas 7704
(Received 21 March 1995)

ac flux-profile measurements are used to determine the current density j, the reversible penetration depth λ' of a pinned flux lattice, and the reversible displacement d, which is the distance flux can move before being unpinned. Both parameters λ' and d describe the elastic regime of the interaction between vortices and defects whereas the current corresponds to the maximum elastic or plastic distortion. The influence of thermal relaxation on these parameters and on ac measurements in general is discussed. Anomalous features of the flux profiles observed in various low-T_c superconductors are correlated with the saturation of the current based on plastic deformation of the vortex lattice. A comparison with flux profiles from single-crystalline and melt-textured $YBa_2Cu_3O_{7-\delta}$ shows the same anomalous feature. This demonstrates the importance of plastic shear also in high-T_c superconductors which seems to be present in the whole magnetic-field regime. Collective pinning and the related peak effect of the current in V_3Si are compared with the fishtail effect in $YBa_2Cu_3O_{7-\delta}$ single crystals. The different magnetic-field dependences of λ' and d in the region of maximum current point to differences between these observations. Decreasing current correlated with decreasing λ' in specimens with a fishtail are related to a softening of the vortex lattice at fields below the maximum current. This anomalous feature is not observed in samples with a current continuously decreasing with magnetic field.

I. INTRODUCTION

The current density j that is carried by a superconductor at tolerable low electric fields E is a crucial parameter for a variety of possible applications in high-T_c materials. Investigations of the current dependence on the electric and magnetic field B and temperature T have not yet resulted in a consistent pinning model for j neither in low-T_c (LTSC), nor in high-T_c superconductors (HTSC). One main problem is the correlation between j and the defect structure of the material which pins the vortex lattice and—for the theoretical modeling especially—whether this interaction leads to elastic or plastic deformation of the vortex lattice. This information is of basic importance for any pinning model. A weak discrimination between both mechanisms may be obtained from the magnetic-field dependence of j and its saturation behavior, i.e., about constant current despite increasing strength of the defect structure as investigated in a variety of LTSC.[1–4] Other pinning parameters offer more direct information concerning this and other problems of the pinning phenomenon. One of them—the reversible penetration depth λ' describes the characteristic length within which a distortion of the pinned flux lattice decays.[5] This length becomes smaller with increasing strength of the pinning interaction and with decreasing vortex-vortex interaction, opposite to the behavior of j. Upper and lower limits of this quantity are the sample size and the London penetration depth, respectively. The reversible penetration depth can be measured from the ac response of the superconductor to an ac magnetic field with sufficiently small amplitude.

The second parameter is the reversible displacement d which represents the distance of reversible motion of the vortices within the effective pinning potential.[6] This length corresponds to the linear part of the force displacement curve of pinned vortices and reflects approximately the displacement before vortices become unpinned or the size of the potential. The reversible displacement is related to the Labusch parameter α, i.e., the slope of

the restoring force in the linear regime, and to the equation

$$j = Bd/(\mu_0 \lambda'^2) \ . \tag{1}$$

The value can be measured from the ac-induced voltage, from ac transport current,[7] or it may be calculated from Eq. (1) if j and λ' are measured. The ratio d divided by the mean distance between vortices a is expected to be about constant as long as the pinning interaction does not change. In LTSC d/a was found to be in the region between 0.5 and 0.1. The larger value is expected in the direct summation limit for elementary pinning forces or in the case where plastic shear between vortices determine j whereas the lower value is related to collective pinning. The value d/a decreases if the elastic interaction between vortices dominates.[8–10] A comparison of these parameters between LTSC and HTSC allows one to study the influence of properties specific to HTSC as short coherence length, large anisotropy, and high temperatures on the pinning interaction. Based on results from LTSC it allows further to check high-T_c pinning models not only by investigating the current.

In this paper we discuss measurements of j and λ' on NbTi, V_3Si, $PbMo_6S_8$, and on $YBa_2Cu_3O_{7-\delta}$. In Sec. II some experimental details about samples and measurements are given. In Sec. III we investigate the influence of thermally activated relaxation on ac magnetic measurements with respect to the determination of j and λ'. It is shown that the rearrangement of flux caused by the ac field is not determined by the $E(j)$ characteristics because the time-dependent electric field at the surface is not in equilibrium with the current inside the sample. A comparison of j, λ', and d/a between LTSC and HTSC is made in Sec. III. Conclusions concerning plastic flow of the vortex lattice and the relation between the $j(B)$ "peak effect" in LTSC and the "fishtail" in HTSC are discussed.

II. EXPERIMENTAL

Magnetic flux-profile measurements were made on various LTSC and HTSC samples by an ac method after Rollins *et al.*[11] In the nonlinear $E(j)$ regime this method allows us to obtain the radial distribution of j and at certain conditions the reversible penetration depth of a pinned flux lattice λ' and the corresponding reversible displacement d. As in all measurements of magnetic moments the length scale must be known within which the induced shielding currents flow. In the investigated nongranular LTSC and HTSC single crystalline and melt-textured $YBa_2Cu_3O_{7-\delta}$ this is the macroscopic sample size. An ac magnetic field was applied and the change of flux was detected by a pickup coil. This induced voltage which corresponds to reversible and irreversible motion of vortices was measured as a function of time with a transient recorder. The measurements were made at frequencies f between 1 Hz and 1 kHz at magnetic fields sufficiently below the irreversibility field where ac losses from flux flow can be neglected. A part of the reversible signal results from the region in the sample where the change of the ac field is too small in order to unpin the vortex lattice. The irreversible part is due to the hysteretic losses of the vortices changing the flux gra-

TABLE I. Survey of the measured specimens.

Specimen	Preparation	Ginzburg-Landau parameter	Upper critical or irreversibility field
NbTi	Nb 49 weight % Ti, cold drawn to 1.1 mm in diameter, area reduction 10^4, heat treated at 380 °C for 10 h.	≈ 70	$B_{c2} \approx 10.4$ T at 4.2 K
V_3Si	Single crystals, annealed at 1800 °C for 3 weeks, irradiated with fast neutrons at different fluences Φt.		
(1)	$\Phi t = 2 \times 10^{22}$ m^{-2}	29.6	$B_{c2} \approx 11.6$ T at 11.3 K
(2)	$\Phi t = 2 \times 10^{19}$ m^{-2}	17.3	$B_{c2} \approx 5.6$ T at 13.5 K
$PbMo_6S_8$	Polycrystalline bulk material	≈ 100	$B_{irr} \approx 11.6$ T at 10 K
$YBa_2Cu_3O_{7-\delta}$		≈ 100	
(1)	Stack of 10 single crystals		$B_{irr} \approx 3.8$ T at 77 K
(2)	Melt-textured bulk material with 211 precipitates		$B_{irr} \approx 6.8$ T at 77 K
(3)			$B_{irr} \approx 5.9$ T at 77 K

dient from one sign to the opposite. Based on the critical state with a steplike voltage current characteristics a calculation of the flux profile from the measured induced voltage versus time results in a curve which is not a straight line through the origin as expected for homogeneously distributed pinning centers. The unexpected flat part at the surface of the profile represents the reversible penetration depth λ' and is caused by the purely reversible signal just after the external ac field $b(t)$ changes the sign of derivative db/dt. With increasing ac field the irreversible motion dominates resulting in a straight line for larger distances from the surface. The gradient of this part of the flux profile corresponds to the current density. Accompanying measurements were made on the same specimens with a vibrating sample magnetometer (VSM) (Oxford 3001), in order to obtain $E(j)$ characteristics from the normalized creep rate and the time constant τ which describes the rearrangement of flux after a change of the electric field E at the surface of the sample. Both ac flux profile and VSM measurements were made on cylindrical specimens at which the applied ac and dc fields were directed parallel to the cylinder axis. For the investigations of the single crystalline $YBa_2Cu_3O_{7-\delta}$ we used a stack of ten crystals from the same batch with typical size $2\times2\times0.3$ mm. The crystals were mechanically processed into a cylindrical shape of 1.5 mm in diameter. After this they were measured separately by VSM in order to select samples with a variation of j and of the irreversibility field B_{irr} less than 10%. The melt-textured samples had a cylindrical shape of 2–3 mm along the c axis and about 1 mm^2 area in the ab plane. Both fields were aligned along the c axis resulting in induced shielding currents flowing within the ab plane of the crystals. The LTSC specimens were of cylindrical shape with diameters of 1–2 mm and several mm in length. Table I gives a survey of the measured specimens.

III. RESULTS AND DISCUSSION

A. Flux profile and reversible penetration depth

In the first part of this section we discuss general problems of determining pinning parameters from ac magnetic flux-profile measurements. We assume a cylindrically shaped specimen with radius R, the parameter x corresponds to the distance from the surface. The position and time dependence of the electric field $E(x,t)$ is determined by the applied ac magnetic field $b(t)$ at the surface and by the penetration depth of the ac field $x(t)$. If the maximum penetration depth is much smaller than the radius: $x(T/2)/R \ll 1$ the electric field in the region $0 \le x \le x(t)$ is approximately obtained from the equation: $E(x,t)=(db/dt)(x(t)-x)$.

The penetration depth $x(t)$ is given by the electric-field dependence of the current and its radial distribution $j(x,E)$. Because the experimental results show a position-independent current, i.e., no surface barrier or surface pinning, we discuss in the following only the case of a homogeneous current density.

We assume first a steplike voltage-current characteristics: $E=0$ for $j \le j_c$ where j_c is the critical current density without thermally activated depinning. For a powerlike approximation $E(j)=E_c(j/j_c)^n$ this corresponds to an infinite exponent n. The related voltage in the superconducting state induced in the pickup coil is

$$U_s(t)=U_{nc}(t)\{1-[1-x(t)/R]^2\} \quad (2)$$

with $U_{nc}(t)\sim(db/dt)\,\pi R^2$ representing the induced voltage in the normal conducting state where the skin penetration depth is much larger than R.[11] From the measured $U_{nc}(t)$ and $U_s(t)$ $x(t)/R$ can be calculated and the flux profile $B(x/R)$ is reconstructed plotting $B(x(t))$ versus $x(t)/R$ with t as parameter $B(x(t))$ is obtained from the symmetry of the flux profile: $B(0,t)-B(x(t))=B(x(t))-B(0,0)$ which can be checked experimentally by comparing $U_s(0\le t\le T/2)$ with $U_s(T/2\le t\le T)$. The schematic drawing in Fig. 1 shows $B(x/R)$ for $t=0$, $t=T/2$ and for a time t with $T/4<t<T/2$ (thick line).

This picture must be modified because if flux lines become unpinned by the change of the direction of the Lorentz force at $x(t)/R$ they must move a finite distance in order to become pinned and to build up the critical state again. This means that the conversion from j_c to $-j_c$ at $x(t)/R$ needs a characteristic length which is given by Campbell's reversible penetration depth λ'. The corresponding reversible induced signal $U_{rev}(t)$ results from the area around $x(t)/R$. In the time interval $0\le t\le t_{rev}$ no irreversible signal is present. The field $b(t_{rev})$ is the amplitude at which irreversibility starts. The corresponding change of the flux profiles is schematically shown by the dotted lines in Fig. 1. The measurable induced signal $U_i(t)$ is the superposition from $U_s(t)$ and $U_{rev}(t)$. For $0\le t\le t_{rev}$ no irreversible flux movement occurs, $U_s(t)$ is zero up to t_{rev}, and the obtained flux profile using $U_i(t)$ in Eq. (2) shows zero current in this

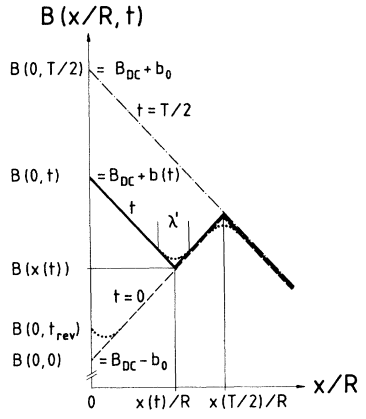

FIG. 1. Schematic drawing of the flux-profile magnetic field B vs distance x from the surface normalized by the sample radius R. The applied field is the stationary field B_{dc} plus the ac field $b(t)$. The thick line represents the flux profile for increasing $b(t)$ at the time t. The momentary penetration depth of the ac field is given by $x(t)$. The dashed and the dashed-dotted line correspond to the profiles at $t=0$ and $t=T/2$, respectively. The dotted lines represent the changes if the response of the elastic regime of the interaction is considered.

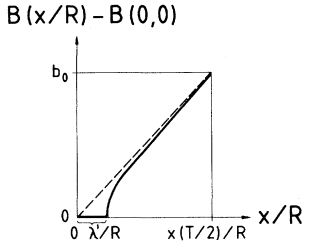

FIG. 2. Calculated flux profile (thick line) with consideration of the elastic response from the reversible flux movement within λ'. The current density j_c is assumed to be independent from x and to follow steplike $E(j)$ characteristics at $j=j_c$.

time interval. This corresponding flat part in Fig. 2 is equal to λ'/R. With increasing penetration depth $U_s(t)$ dominates in comparison to $U_{\rm rev}(t)$ and the flux profile approaches towards the result from the pure irreversible flux motion (dashed line in Fig. 2). A more realistic case must assume irreversible flux motion also for fields below $b(t_{\rm rev})$ for reasons which are discussed below. In this case the slope of $db/d(x/R)$ for $0\le x\le\lambda'$ is not zero and it does not become infinite at $x=\lambda'$.

The next step is to consider thermally activated relaxation of the pinned flux lattice. This influence on the flux-profile measurement may be divided into two parts: finite exponent n which changes U_s and an additional voltage $U_{\rm Th}$ from flux movement. The first part is due to the finite steepness of the voltage-current characteristics which results in a current density j smaller than j_c for the same electric field at a constant position x. The time structure of the applied ac field itself becomes important because it determines E and results in a time-dependent current density. The dashed line in Fig. 3 represents as before $n=\infty$ from Fig. 1, whereas the thick line corresponds to a flux profile with a finite n. At $t=0$ and $t=T/2$ db/dt becomes zero and the penetration depth $x(t)/R$ increases in comparison to the unrelaxed case. Zero db/dt does not mean $j=0$ because as discussed below $E(j)$ of the flux profile is not in an equilibrium state like in a free transient decay of a magnetic moment from an induced shielding current. Besides, in the approximate calculation of $x(t)/R$ in the case of a finite steepness of $E(j)$, a second problem arises from the calculation of $B(x(t))$ because the flux profile becomes asymmetric with respect to $B(x(t))$.

The second part that influences the flux-profile measurement results from relaxation of the flux profile. The flux front decays and induces a signal $U_{\rm Th}(t)$ which does not follow the time structure of the applied ac field. Especially $U_{\rm Th}$ becomes a maximum at $t=0$ or $t=T/2$ where the region of the decay extends from the surface up to the maximum penetration depth. The signal $U_{\rm Th}$ has opposite sign as U_s and $U_{\rm rev}$ and causes a shift Δt of the time between $U_{\rm nc}(0)=0$ and $U_i(\Delta t)=0$. The related flux profile from measured $U_i=U_{\rm rev}+U_s+U_{\rm Th}$ is schematically shown in Fig. 4. The finite field at the surface results from using Eq. 2 for $U_i\ge 0$ at $t\ge\Delta t$ and corresponds to $[B(0,\Delta t)-B(0,0]/2$. This value reflects therefore an indirect measure of thermally activated flux movement. The phase shift Δt and the signal $U_{\rm Th}$ $(t=0)$ which can be measured were related by Kerchner[12] to thermally activated flux creep based on the Anderson-Kim[13] model. Using Eq. (17) and (23) of Ref. 12 we calculated from the measured $U_{\rm th}(t=0)$ and Δt the normalized creep rate S and compared these data with those obtained from a free transient decay of the shielding current measured with a vibrating sample magnetometer $S(\mathrm{VSM})=j^{-1}(dj/d\ln t)$. Figure 5 shows $S(U_{\rm th})$ values from $U_{\rm Th}(t=0)$ which are one order of magnitude smaller than $S(\mathrm{VSM})$ from the time-dependent decay of j. This difference cannot be related to the different electric fields used for the measurements [$E\approx 0.04$ μV/cm (VSM) and $E\approx 1$ μ/cm (flux profile)]. It demonstrates that the flux-profile decays much slower than expected from a free transient decay. The flux profile between $x(t)$ and $x(T/2)$ is not in equilibrium with the electric field at the surface. The redistribution of flux towards this equilibrium state is governed by the time constant τ.[14] In the time region $0\le t\le\tau$ redistribution of flux dominates and the decay of j is much slower than in the equilibrium state for $t\gg\tau$. Because the ac measurements were done in the time regime $t<\tau$ we expect lower influence of relaxation in accordance with $S(\mathrm{VSM})>S(U_{\rm Th})$ from Fig. 5. This was further proved from a comparison between the τ values measured with a VSM and the characteristic time $T=f^{-1}$ of the ac field. The inset of Fig. 6 shows how τ is obtained from a measurement of the magnetic moment m vs t for $E=2\times10^{-5}$ μV/cm. Figure 6 shows

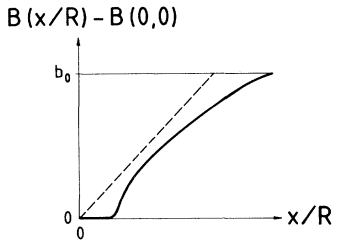

FIG. 3. Schematic drawing of a calculated flux profile (thick line) with the same assumptions as in Fig. 2 but replacing the steplike $E(j)$ characteristics by a $E(j)$ with finite steepness.

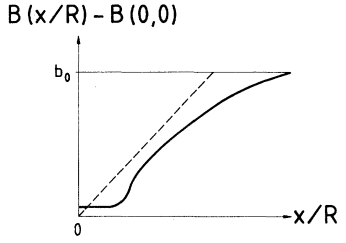

FIG. 4. Schematic drawing of a calculated flux profile (thick line) with the same assumptions as in Fig. 3 but taken into account an induced signal from thermally activated flux movement.

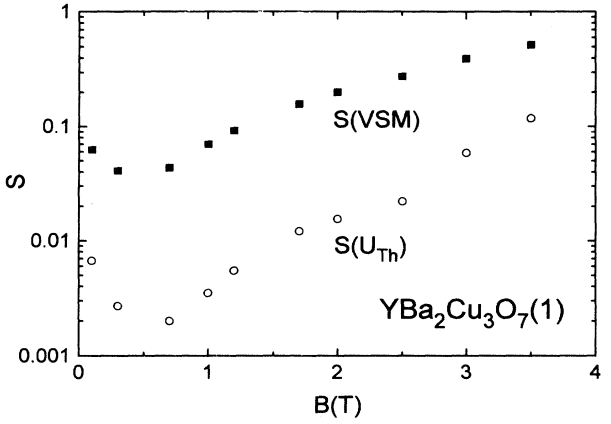

FIG. 5. Normalized creep rate $S=j^{-1}(dj/d\ln t)$ vs B from measurements with a vibrating sample magnetometer S(VSM) and from the measured voltage $U_{\rm Th}$. The value $S(U_{\rm Th})$ is related to flux creep of the ac-induced flux profile. The measurements are made at 77 K.

$\tau(B)$ for $E=0.2$ μV/cm based on the proved relation $\tau=K(dm/d\ln t)/E$ with K representing a geometry factor.[15] The dashed line which corresponds to $T/2$ for a frequency of 100 Hz ($E=0.2$ μV/cm) is clearly below τ. This holds for all frequencies because the ratio τ/T is independent of E, i.e., a change from $t<\tau$ to $t>\tau$ can only be realized by a variation of $dm/d\ln t$ with magnetic field or temperature. At 77 K this occurs for $B>3$ T where $dm/d\ln t$ and therefore τ becomes sufficiently small. In this case $U_{\rm Th}$ from relaxation results predominantly from the time regime $t>\tau$, in accordance with Fig. 5 where $S(U_{\rm Th})$ becomes comparable to S(VSM) at higher magnetic fields. In the vicinity of the irreversibility line where the current approaches zero, naturally the region $\tau \ll t$ is reached and both S values should be the same.

But if ac measurements are made in the time region $t<\tau$, as in this work, the related creep rates do not correspond to those from magnetization measurements made at $t \gg \tau$.

Both contributions from relaxation influence the determination of j and λ' differently. The error of the j value is small if the gradient of the flux profile is taken from its steepest part at about $t=T/4$ where E approaches its maximum and U_s dominates. In this case also sinusoidal and triangular ac fields result in very similar j values for the same ac amplitude and frequency. The frequency dependence may be used for the determination of $E(j)$ characteristics as shown in Fig. 7. The influence from relaxation on λ', however, is much more severe because this parameter is obtained from the time region of pronounced thermal flux movement. The time dependence of the corresponding signal $U_{\rm Th}(t)$ cannot be calculated and therefore no analytical separation between $U_{\rm rev}(t)$ and $U_{\rm Th}(t)$ is possible at the present stage. Also the frequency or E dependence of λ', as shown in Fig. 7, does not allow to account for the relaxation influence. This $\lambda'(E)$ relation is governed by the E dependence of j, d, and $U_{\rm Th}$ from which only $j(E)$ can be measured. The measurements shown in Fig. 7 give approximately $j\sim E^{1/3}$, $\lambda'\sim E^{-1/3}$, and therefore $j\sim\lambda'^{-1}$. This result contradicts Eq. (2) and demonstrates the importance of the unknown E dependence of d and $U_{\rm Th}$. It should be mentioned again that only $U_{\rm Th}(t=0,E)$ can be measured but not its time dependence. For this reason we used an indirect method to recognize the influence of relaxation on λ'. We compared flux profiles from a sinusoidal—and from a triangular applied ac field obtained with the same frequency and amplitude, this means with the same current. The measured $U_{\rm Th}$ at $t=0$, shown in Fig. 8, reveals large differences demonstrating different relaxation rates in both measurements. Therefore different λ' values obtained from sinusoidal or triangular ac fields are expected if $U_{\rm Th}(t=0)$ from relaxation does not become

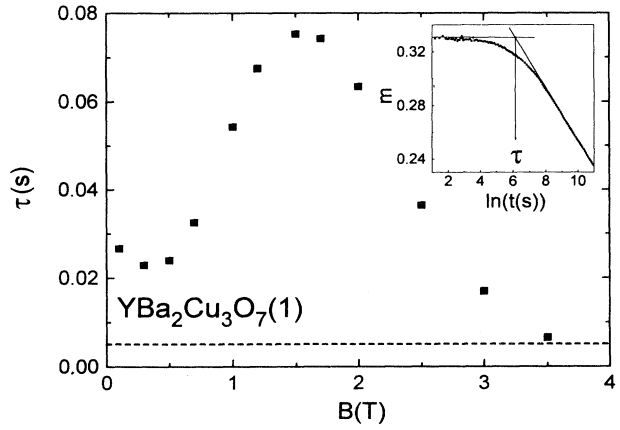

FIG. 6. Time constant τ vs B at 77 K for an electric field of $E=0.2$ μV/cm. The dashed line indicates half the time period of the frequency $f=100$ Hz which is equivalent to 0.2 μV/cm at the sample surface. The inset shows a measurement of magnetic moment vs $\ln t$ at $T=77$ K, $B=1$ T, $E=2\times10^{-15}$ μV/cm from which τ is obtained.

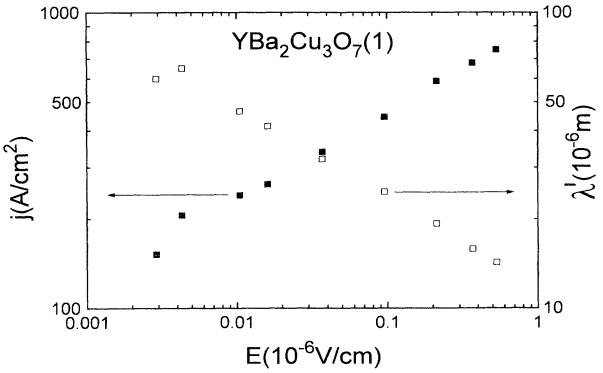

FIG. 7. Current density j and reversible penetration depth λ' vs electric field E obtained from a variation of the frequency between $f=1$ Hz and 1 kHz but constant ac amplitude. The measurements, shown for 77 K, 3 T, are not consistent with $j\sim\lambda'^2$ which points to the influence of $d(E)$ and $U_{\rm Th}(t,E)$. Measurements at lower B fields come closer to $j\sim\lambda'^2$ in agreement with steeper $E(j)$ characteristics.

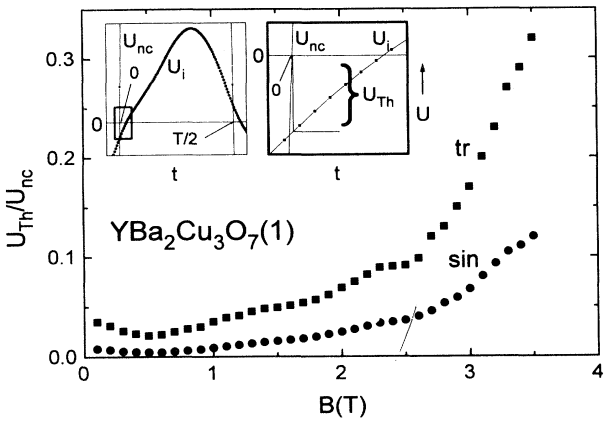

FIG. 8. Voltage U_{Th} at the time were the derivative of the applied ac field is zero vs B at 77 K. The values are normalized with the amplitude of the voltage in the normal conducting state U_{nc}. The measurements are made with a triangular (tr) and a sinusoidal (sin) applied ac field with the same frequency and amplitude. The insets show $U_i(t)$ at $T=77$ K, $B=1.7$ T and $U_{nc}(t)$ for a sinusoidal applied ac field. On the time scale the arrows indicate $t=0$ and $t=T/2$. The right inset is an amplification of the area around $t=0$ from which $U_{Th}=U_i(t=0)$ is obtained.

negligible. Figure 9 shows the ratio λ' obtained from a triangular ac signal divided by the value from a sinusoidal signal. This ratio is about 1.1 and remains constant in the magnetic-field regime up to 2 T where the exponent n is still above 5. At higher fields the ratio increases because relaxation becomes more pronounced and influences the determination of λ'. For this reason we restrict our discussion on λ' to the B,T region with $n>5$ where the influence of relaxation is still a small perturbation. The λ' values become larger if relaxation increases especially with increasing $U_{Th}(t=0)$. For a triangular ac field $U_{Th}(t=0)$ is always larger (Fig. 8) because the constant db/dt prevents a smooth approach towards the equilibrium state at $t=0,T/2$ as in the case for a sinusoidal field with db/dt approaching zero. The n values in Fig. 9 were obtained from a power-law approximation of the $E(j)$ characteristics.

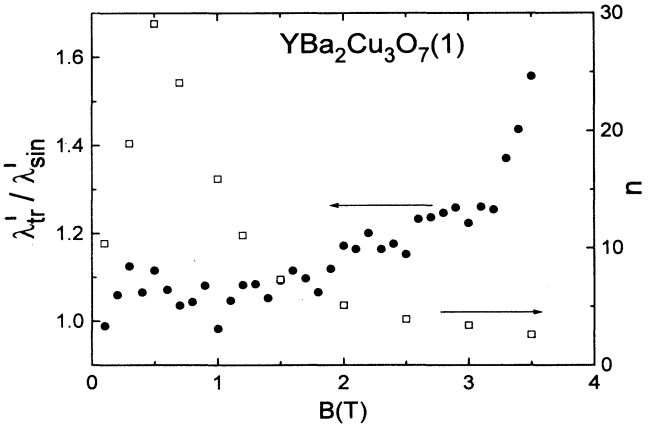

FIG. 9. Ratio of the reversible penetration depths from a triangular and from a sinusoidal applied ac field $\lambda'_{tr}/\lambda'_{sin}$ vs B at 77 K (filled circles). The open squares show the exponent n of the voltage-current characteristics $E\sim j^n$.

Flux profiles in HTSC investigated so far do not show the shape as expected from Fig. 4. The signal in the region $0\le x\le\lambda'$ is not completely reversible which results in a finite slope of $db/d(x/R)$ for $x<\lambda'$ and in a less pronounced change of the slope at $x=\lambda'$. As an example flux profiles from a single crystal $YBa_2Cu_3O_7$ (1) at 77 K are shown in Fig. 10. The arrow indicates the λ' value determined from an extrapolation of $b(x)$ to $b=0$ in the region of maximum slope $db/d(x/R)$. But also LTSC show only in certain B and T regions the predicted flux profiles. In all investigations made in well characterized homogeneous low-T_c specimens the shape of the flux profiles change continuously with increasing B or T from the expected shape to a shape very similar as in $YBa_2Cu_3O_{7-\delta}$. Figures 11(a)–11(c) demonstrate this for NbTi, for fast neutron-irradiated V_3Si and for $PbMo_6S_8$. Flux profiles at the lowest reduced field shown in Figs. 11(a)–11(c) correspond to the expected shape, in contrast to the larger reduced fields at which the anomalous behavior becomes more pronounced with increasing field. As mentioned above the unusual feature is the nonzero slope of $db/d(x/R)$ in the region $0\le x\le\lambda'$. In the following we discuss possible explanations for the deviation from the expected shape of the flux profile.

(1) Relaxation as a first possibility can be rejected as being the main reason based on the comparison between Figs. 8 and 9 and the corresponding discussion above: different relaxation rates between triangular and sinusoidal applied ac field do not result in different λ' values or different slopes for $0\le x\le\lambda'$.

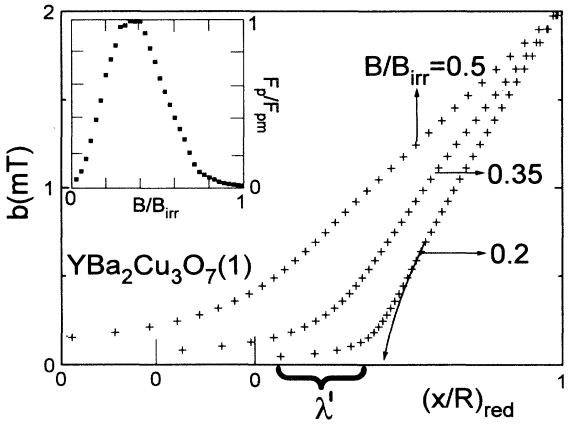

FIG. 10. Flux profiles $B(x/R)$ at 77 K measured at different reduced fields B/B_{irr} with an ac amplitude of $b=5$ mT and a frequency of 312 Hz. The distance x from the surface is normalized with the radius R of the sample and with the penetration at $b=2$ mT. For clarity the surface $(x/R)=0$ is shifted for $B/B_{irr}=0.35$ and 0.2 to different positions on the abscissa. The value $b=0$ corresponds to the stationary field B. The inset shows the volume pinning force reduced with its maximum value versus reduced field B/B_{irr}.

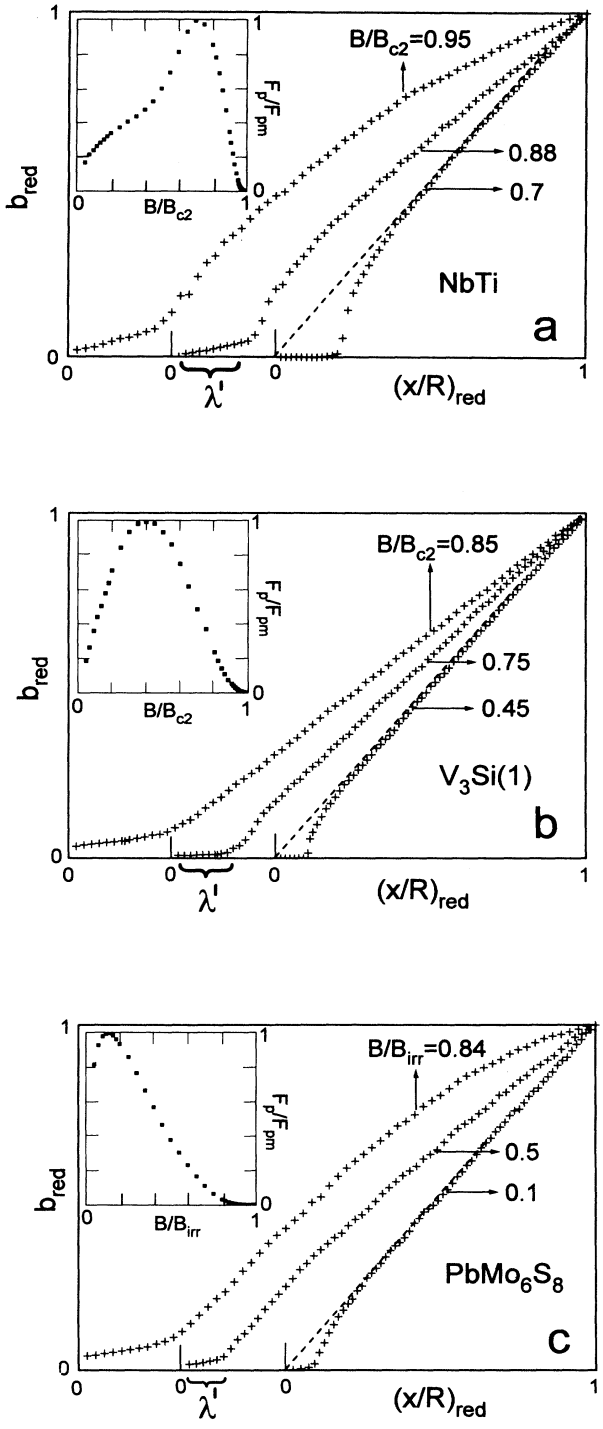

FIG. 11. (a)–(c) Flux profiles $B(x/R)$ measured at different reduced fields. The temperatures as well as B_{c2} and B_{irr} are given in Table I. The ordinate is normalized with the ac field, $b_{red}=0$ corresponds to the stationary field B. The distance x from the surface is normalized with the radius R of the sample and with the penetration at a certain applied ac field. $(x/R)_{red}=1$ does not correspond to the maximum penetration of the ac field. The insets give the volume pinning force reduced with its maximum value versus reduced field.

(2) An inhomogeneous surface layer with a lower j than the bulk value offers a straightforward explanation. But it can be excluded for the LTSC in Figs. 11(a)–11(c) as well as for the studied $YBa_2Cu_3O_{7-\delta}$ specimens. In all these investigations λ' values vary as a function of B or T by more than one order in magnitude. This would require a variation of the thickness of the hypothetical surface layer in quite the same way which makes this possibility very doubtful. Further the obtained j, λ', and d values are consistent with Eq. (1), i.e., $j\sim\lambda'^{-2}$ is roughly fulfilled which also makes a correlation between λ' and an inhomogeneous region at the surface very improbable.

(3) A third possibility may result from a granular behavior of the current. In this case decoupling between the quite different inter- and intragrain current densities causes a change of the slope $db/d(x/R)$ if the intergrain screening capability is exhausted. The lower intergrain current, from the surface up to the field where the intergrain screening is saturated may also lead to a misinterpretation of λ'. But the same arguments used for the discussion of the surface layer are also suitable for an exclusion of this possibility. Further magnetic and transport current measurements of the studied HTSC specimens rejected directly a decoupling.[16,17]

(4) An increase of the reversible signal, more than expected from the measured current density was observed in the geometry $B\|a,b$ in melt-textured $YBa_2Cu_3O_{7-\delta}$.[18] These larger λ' values were related to the presence of internal surfaces from cracks. However, it was demonstrated that this explanation is not applicable for the geometry $B\|c$ in the present investigated melt-textured $YBa_2Cu_3O_7$ specimens.[17]

(5) A distribution of the elementary pinning forces may lead to a depinning of flux lines at pinning sites with a lower force. This results in an irreversible flux movement at distances below the average λ' values. But also, this possibility becomes questionable from the observation that distorted flux profiles in LTSC are only observed in a certain field region as discussed in detail below.

(6) An irreversible behavior of a part of the flux lattice within the region of global reversible motion[19] may result from plastic deformation of the flux lattice if locally the shear force becomes smaller than the pinning force.

Weakly interacting pointlike defects in the presence of stronger pinning centers in HTSC and the large Ginzburg-Landau parameter κ favoring the presence of flux-lattice defects and decrease the shear force of the flux lattice in comparison to the pinning force. Both support the last explanation as the dominating reason for the unexpected flux profiles. This holds also for the low-T_c specimens where a transition from an elastic distorted flux lattice to a plastic distortion were proved by history effects and found just in the region below the maximum volume pinning force where the flux profiles changed their shape. In $PbMo_6S_8$ with κ similar to $YBa_2Cu_3O_{7-\delta}$, even at very low fields the flux profiles do not become regular [Fig. 11(c)] comparable to the HTSC. Further one expects a less pronounced dependence of the current on the properties of the defect structure if the Lorentz force is balanced by the shear force of the flux lattice. Such a saturationlike behavior, related to plastic defor-

mation, is observed in the LTSC of Figs. 11(a)–11(c).[4,10,20,21] The influence of saturation is restricted to the higher-field region where the shear modulus of the flux lattice and the related shear force decrease faster with B than the pinning force. Below the maximum of the volume pinning force $F_p = B \cdot j$ the depinning process determines the current which results in a normal flux profile. The insets in Figs. 11(a)–11(c) show the reduced volume pinning force vs reduced field for the three LTSC specimens. Above the maximum of F_p at which the defect structure is of lower influence due to plastic deformation, the flux profile starts to deviate from the ideal shape. Transferring this correlation between plastic deformation and unusual flux profile to the HTSC, it indicates that in the $YBa_2Cu_3O_{7-\delta}$ specimens plastic deformation of the flux lattice is present in the whole B and T area similar as in $PbMo_6S_8$. This mechanism may not dominate but besides the depinning it influences the behavior of the current. This is also in accordance with the absence of history effects in $YBa_2Cu_3O_{7-\delta}$ and $PbMo_6S_8$ wires because there is no change from plastic to elastic distortion of the flux lattice. Further the saturation of j in HTSC correlated with plastic deformation was partly observed and discussed.[22–25]

B. Comparison of pinning parameters between low- and high-T_c superconductors

In this section we investigate pinning parameters and their relation to pinning models especially to the origin of the fishtail in $YBa_2Cu_3O_{7-\delta}$. A general discussion of this phenomenon and the influence of the oxygen content is given in Ref. 24. The measurements on $YBa_2Cu_3O_{7-\delta}$ are made with 30 Hz whereas 11.6 Hz were used for investigating V_3Si. The variation of the electric fields from the different frequencies and sample sizes is of negligible influence on the results due to the sufficiently large steepness of the $E(j)$ characteristics. Figure 12 shows $\lambda'(B)$ determined from the flux profiles and the ratio reversible displacement divided by the mean flux distance d/a obtained from Eq. (1). The measurements of Fig. 12 are made on a melt-textured sample $YBa_2Cu_2O_7$ (2), showing a continuously decreasing current density with B. The reversible penetration depth is in the region of some μm, one order in magnitude larger than the London penetration depth. The λ' values obtained from the flux profile are slightly overestimated mainly due to the influence of plastic deformation and relaxation as mentioned above. This means that d or d/a values calculated from Eq. (1) represent an upper limit. The d/a ratios at higher B are below 0.02 which corresponds to absolute d values of some nm, comparable to the coherence length. These very small reversible displacements in comparison to the flux distance point to core pinning interaction of dense, point-defect-like pinning centers. This is not in contradiction to plastic deformation of the flux lattice because this mechanism is not expected to be dominant but occurs locally and is only visible at flux-lattice movements below λ'. Similar small displacements were observed in melt-textured and thin films of $YBa_2Cu_3O_{7-\delta}$.[7,17,27–29] The magnetic-field, and temperature dependence of λ' in $YBa_2Cu_3O_7$ (2) behave normally as expected from all observations in LTSC: both λ' and j show opposite behavior—decreasing $j(B,T)$ is correlated with increasing $\lambda'(B,T)$ and vice versa.

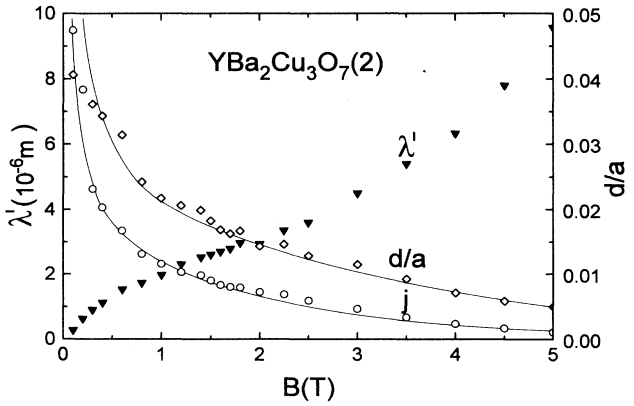

FIG. 12. Reversible penetration depth λ', reversible displacement d divided by the flux distance a and the current density j vs magnetic field B at 77 K. j is given on a linear scale between 0 and 1.4×10^5 A/cm^2, the scale is not shown for clarity.

In the following we summarize briefly measurements of j, λ', and d on V_3Si made as a function of B,T and pinning center density N. Results and discussion of these investigations which are partly published in Refs. 9, 20, and 21 shall be used for a comparison with the HTSC specimens. The V_3Si crystals irradiated with fast neutrons show below a certain magnetic-field and defect concentration a satisfying agreement with the collective-pinning theory of Larkin and Ovchinnikov.[30] The weakly interacting pointlike pinning centers cause elastic deformation in the flux lattice which is accompanied by low currents and a slowly decreasing d/a with B similar to that in Fig. 12. However, a smooth variation of d/a is not expected if the pinning mechanism changes as for instance in the region where single-vortex pinning becomes influenced by vortex-vortex interaction and in the transition region from elastic to plastic deformation of the flux lattice. Above this transition area d/a approaches higher values and decreases further with B towards B_{c2}. Such a typical behavior is shown in Fig. 13 for V_3Si (2) with a j vs B peak. The regime of single-vortex interaction with a constant slope of the restoring force per flux line vs displacement $d(j\phi_0)/du$ is probably observed below 0.5 T. The transition to the regime where plastic flow becomes important occurs from 4.3 to 4.6 T. The peak effect of the current at about 4.7 T is correlated with a minimum of λ' and a maximum of d/a. Below the peak all three pinning parameters are roughly consistent with a collective-pinning interaction. The field area above the maximum current shows large d/a values up to 0.4 but it is not in accordance with a direct summation model or with a model based on pure plastic deformation of the flux lattice. This follows for instance from the exponent m of the relation $j \sim N^m$ which becomes a function of B and decreases from $m \approx 2$ to $m < 0.1$ if B ap-

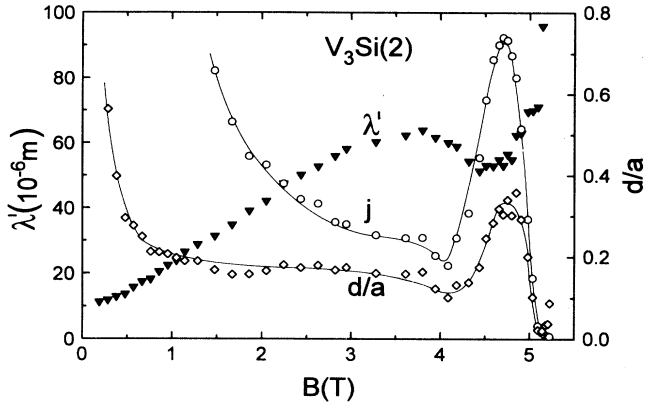

FIG. 13. Reversible penetration depth λ', reversible displacement d divided by the flux distance a and the current density j vs magnetic field B at 13.5 K. j is given on a linear scale between 0 and 900 A/cm^2, the scale is not shown for clarity.

proaches B_{c2}. The field area at which the transition between the two mechanisms takes place shifts with increasing defect density to zero field. This naturally explains the decrease of the peak position to lower fields, further, the height of the peak increases and the shape of the peak broadens. Above a certain N the transition area has vanished and the current density decreases continuously with magnetic field. Figure 14 shows the corresponding measurements of the crystal V_3Si (1) after an increase of the defect density by a factor of 10^3. In contrast to the crystal V_3Si (2) with the lower defect density the d/a values increase with B and reach 0.5 at the broad maximum in the higher-field area. The exponent m decreases from about 1 at low B to 0.1 at $0.9B_{c2}$. This saturationlike behavior which becomes pronounced with B is correlated with the change of the flux profile [Fig. 11(b)] both caused by a more dominating influence of plastic deformation.

A rough comparison between V_3Si (2) in the field region below the $j(B)$ peak and $YBa_2Cu_3O_7$ (2) points to collective pinning also in the HTSC. But relaxation measurements show that collective creep[31] with a negative curvature in log$E$ vs log$j$ is only present in the region of about constant S (Ref. 32) up to $B \approx 2$ T. This indicates that the low d/a values are not necessarily correlated with a collective-pinning interaction. These differences between LTSC and HTSC become even more pronounced if the single-crystal $YBa_2Cu_3O_7$ (1) is compared with V_3Si (2). This HTSC sample has a maximum current at relatively low field. The fishtail effect which is observed in single crystals with dominating point-defect disorder shows the maximum current typical at $B/B_{irr} \approx 0.3$. The about-constant reduced peak position is observed even in quite differently prepared $YBa_2Cu_3O_{7-\delta}$ single crystals. If one expects the same mechanism as for the peak in V_3Si (2) it requires an about-constant defect concentration in the HTSC samples with fishtail. This assumption is less probable and becomes even more doubtful from measurements of crystals with quite different oxygen content, i.e., different concentration of oxygen vacancies, which also show the maximum of the current at the same value B/B_{irr}.[26]

In $YBa_2Cu_3O_7$ (1) (Fig. 15) the expected relation between j and λ' is observed down to 0.5 T, i.e., dj/dB has an opposite sign as $d\lambda'/dB$. However, below 0.5 T this relation has changed, a decreasing current is accompanied by a decreasing λ'. The anomalous correlation between λ' and j leads to the unusual maxima d/a at 0.5 T. This pecularity becomes less pronounced with decreasing temperature. Figure 16(a) shows that the maximum of λ' vanishes at about 50 K whereas the fishtail is still observed at this temperature [Fig. 16(b)]. But the anomalous increase of λ' in spite of increasing j is present at all temperatures. An influence of the self-field for this phenomenon can be excluded because the self-field is smaller than the value at which d/a becomes a maximum.

The peak of d/a in Fig. 15 is further not in agreement with a change from elastic to plastic deformation in the flux lattice as in V_3Si (2) because d/a above the peak ap-

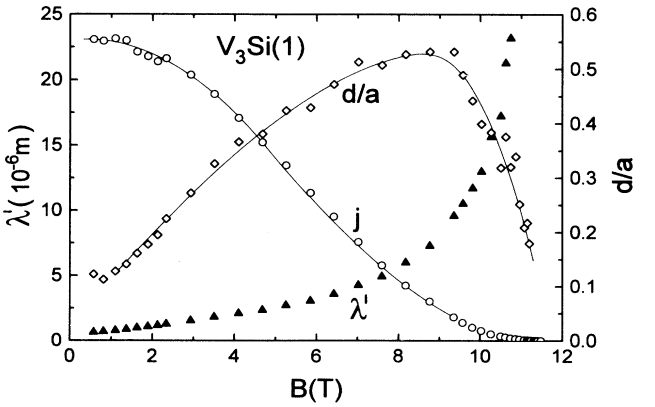

FIG. 14. Reversible penetration depth λ', reversible displacement d divided by the flux distance a and the current density j vs magnetic field B at 11.3 K. j is given on a linear scale between 0 and 8.5×10^5 A/cm^2, the scale is not shown for clarity.

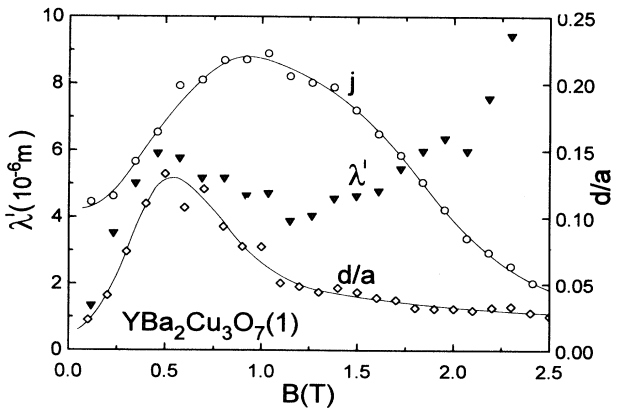

FIG. 15. Reversible penetration depth λ', reversible displacement d divided by the flux distance a and the current density j vs magnetic field B at 77 K. j is given on a linear scale between 0 and 1.75×10^4 A/cm^2, the scale is not shown for clarity.

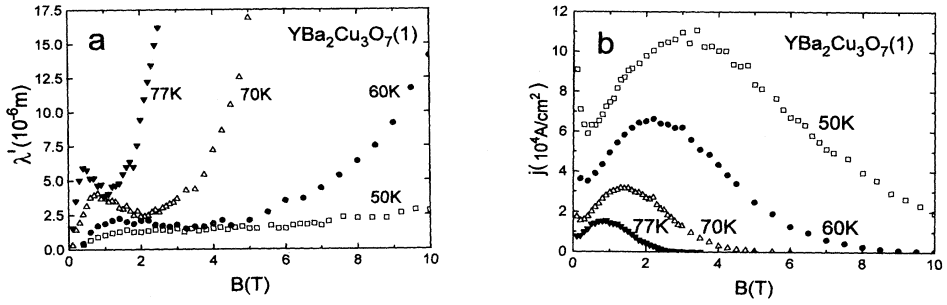

FIG. 16. Reversible penetration depth λ' (a) and current density j (b) vs magnetic field B at different temperatures.

proaches again very small values and the anomalous shape of the flux profiles in $YBa_2Cu_3O_7$ (1) is present in the whole field regime (Fig. 10). Further the peak does not correlate with the maximum current as in V_3Si (2). From these observations we conclude that the fishtail in HTSC may have a somewhat different origin than the peak effect in LTSC. From a comparison between $YBa_2Cu_3O_7$ (1) and $YBa_2Cu_3O_7$ (2), we suggest that the anomalous correlation between λ' and j and the corresponding d/a peak is related to the increase of the current with B. Because this happens at very low fields, where small vortex-vortex interaction is expected, single-vortex pinning or easy flux shear may be involved. In the second case the current is limited by plastic deformation between vortices if the pinning force becomes larger than the shear force between vortices. This may occur either at large fields approaching B_{c2} or the melting point B_{irr} where the elastic moduli decrease or at low fields where vortex-vortex interaction vanishes due to large intervortex distance. A further requirement for a shear limited current is that not all vortices are pinned with the same strength. Such a distribution is always present for dense randomly spaced point pins which interact collectively with vortices. For this reason the current at low fields where vortex-vortex interaction is negligible may be determined by the shear force and not by a single collective interaction. With increasing field the stronger vortex-vortex interaction increases the shear force and the current. This behavior relates the increase of the current with B at low fields to an overcome of the softening of the vortice lattice. The mechanism should occur for weakly interacting defects of high density as in single crystals with impurities or oxygen vacancies. However, a shear limited current is not expected for strongly interacting pins as long as the system does not become dilute, i.e., the distance between flux lines is larger than the spacing between pins. In this field region the current is high and related to a direct summation of the individual interaction forces. At higher fields the system becomes dilute and j may be shear limited or in the presence of point defects it may be related to this current. The transition region between both is indicated by a pronounced decrease of j with B. This behavior corresponds to the melt-textured sample $YBa_2Cu_3O_7$ (2) prepared with 211 precipitates of low concentration. In the dilute case the 211 pinning centers are occupied by flux lines already at very low B. Increasing field results in a pronounced decrease of the current which is then determined by the background pinning of weakly interacting point pinning centers. Such a defect structure of strong widely spaced pins is further in accordance with increasing d/a if B decreases towards the region of single-vortex interaction.

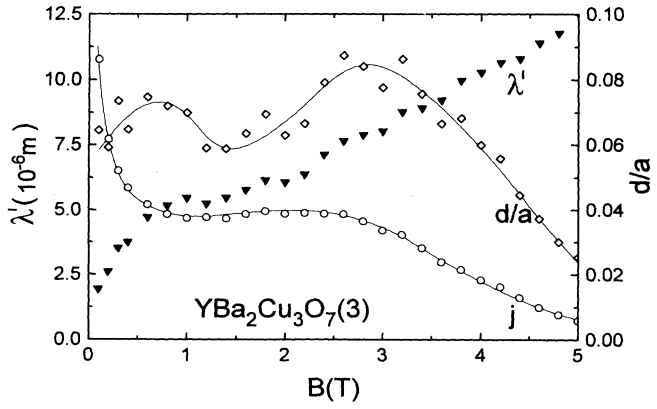

FIG. 17. Reversible penetration depth λ', reversible displacement d divided by the flux distance a and the current density j vs magnetic field B at 77 K. j is given on a linear scale between 0 and 2.2×10^4 A/cm^2, the scale is not shown for clarity.

In single crystals of $YBa_2Cu_3O_{7-\delta}$ with a pronounced fishtail the current decreases down to very low external fields. The increase of j at very low fields [Fig. 16(b)], is related to larger scale defects. An increase of the 211 concentration depresses the $j(B)$ fishtail as well as the specific correlation between j, λ', and d. Figure 17 shows measurements on a melt-textured specimen $YBa_2Cu_3O_7$ (3) with a plateaulike $j(B)$ dependence. The maximum of d/a at about 3 T corresponds as usual in most samples to the maximum of the volume pinning force whereas the roughly constant d/a below 1 T reminds on the possible softening in this area. As shown in Table II, sample 3 shows the fishtail behavior and the $j(B)$ dependence at low fields between $YBa_2Cu_3O_7$ (1) and $YBa_2Cu_3O_7$ (2).

TABLE II. Comparison of data for the three different samples of $YBa_2Cu_3O_{7-\delta}$.

$YBa_2Cu_3O_{7-\delta}$	j(77 K, 0.1 T)	$j(B)$
(1)	7.5×10^3 A/cm^2	Fishtail
(2)	1.6×10^5 A/cm^2	No fishtail
(3)	1.9×10^4 A/cm^2	Plateau

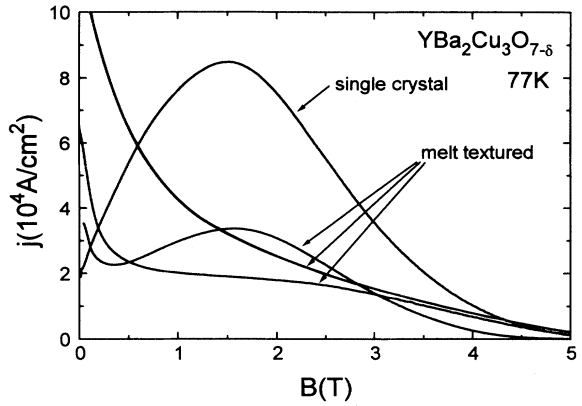

FIG. 18. Current density j vs magnetic field B at 77 K for different melt-textured $YBa_2Cu_3O_{7-\delta}$ and for a $YBa_2Cu_3O_{7-\delta}$ single crystal (different from sample 1) with an irreversibility field similar to other samples.

The suppression of the fishtail effect from the high currents at low B is also demonstrated in Fig. 18 which shows $j(B)$ of different samples with about the same irreversibility field. The depression of the $j(B)$ maximum by large scale defects may result from two possibilities. The presence of defects as for instance 211 precipitates may decrease the density of point pinning centers by enhanced diffusion and segregation. In this case the fishtail vanishes because the necessary defect structure is absent. The second possibility is related to the larger disorder of the flux lattice in the low-field region caused by the softening. The larger scale defects may already produce a disorder in the lattice which prevents a further softening or melting as from the high-density point-defect structure in single crystals.

A final remark is addressed to the Labusch parameter α which is the slope of the force displacement curve in the linear elastic regime. A comparison of the values in Fig. 19 between the three $YBa_2Cu_3O_{7-\delta}$ samples at 77 K suffers from different irreversibility fields and different currents. The α values of sample 2 are in the low-field region about one order in magnitude higher than that one of sample 3 with similar B_{irr} but by a factor of 3 to 5 lower j. At fields above 3 T where the currents become about equal also α of both samples approaches the same values. The field and temperature dependence of α and of $B \cdot j$ is very similar in sample 1, which points to the same interaction mechanism in the entire range of field and temperature. Whereas in samples 2 and 3, this coincidence is not observed. The different dependences of α and $B \cdot j$ on B especially pronounced in sample 2 may be related to different pinning centers dominating at low and high fields, respectively.

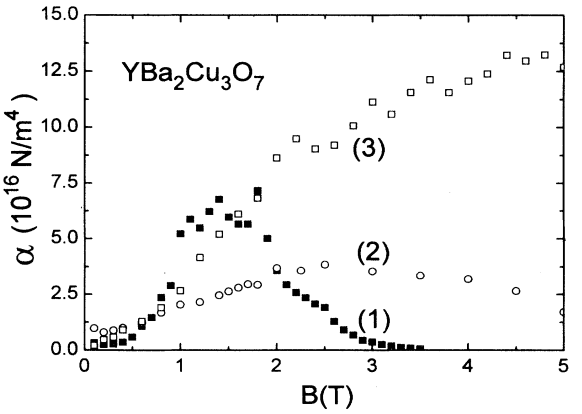

FIG. 19. Labusch parameter α calculated from the relation $B^2/(\mu_0\lambda'^2)$ vs magnetic field B at 77 K. The α values for sample (2) should be multiplied by a factor of 10.

IV. SUMMARY

An ac technique is used to measure flux profiles in various low-T_c superconductors and single crystalline and melt-textured $YBa_2Cu_3O_{7-\delta}$ for the geometry field parallel to the c axis of the crystals. The current density j and the reversible displacement λ' which describes the elastic limit of the interaction between vortices and pinning structure were determined from the flux profile.

The influence of thermally activated flux movement on these parameters is discussed. From the measured induced voltage at the time where the slope of the applied ac field becomes zero, the relaxation rate is calculated. These values are one order of magnitude smaller than relaxation rates obtained from a transient decay of an induced current from VSM measurements. This difference demonstrates that the thermally activated flux motion in an ac experiment is not in equilibrium with the electric field at the sample surface. The measured time constant which describes the rearrangement of flux towards this equilibrium state is much larger than the period of the ac field. This observation means that the equilibrium voltage-current characteristics $E(j)$ do not determine the influence of relaxation on ac measurements made sufficiently below the irreversibility field.

The induced voltage from thermally activated flux motion was observed to be quite different between a sinusoidal and a triangular applied ac field. The influence of relaxation on the determination of λ' was obtained from a comparison between results from both measurements. This influence caused an error of λ' below 20% if the slope of log E vs log$j$ is above 5. Flux profiles at distances from the surface below λ' are expected to have zero slope ($j=0$) because only reversible flux motion should occur in the elastic limit of low driving forces. But the low-T_c specimens show a finite slope in the magnetic-field region at which the current becomes nearly independent from the pinning interaction due to plastic deformation of the vortex lattice. Flux profiles in $YBa_2Cu_3O_{7-\delta}$ revealed the same anomalous feature, but at all magnetic fields, which points to local plastic shear in the region of global reversible flux motion.

A general comparison of λ' between $YBa_2Cu_3O_{7-\delta}$ and LTSC at similar current densities and reduced temperatures shows much smaller λ' values in the HTSC. Consequently the ratio reversible displacement divided by the mean flux distance, d/a, approaches values down to 0.005 whereas in LTSC $d/a \approx 0.1$ represents the lower

limit. This much smaller elastic regime of reversible flux motion results from the dominating interaction with pointlike pinning centers in HTSC. Only $YBa_2Cu_3O_{7-\delta}$ samples with 211 precipitates show larger d/a values at low magnetic fields. The current in samples without such larger scale pinning centers is determined by point defects as in single crystals with a fishtail effect. This maximum current at intermediate magnetic fields is correlated with an anomalous behavior of λ' at fields below the maximum. In all LTSC samples with and without a $j(B)$ peak effect and in $YBa_2Cu_3O_{7-\delta}$ without a fishtail a decreasing current is accompanied by increasing λ' values as expected from vortex-vortex interaction. But in the fishtail sample below the maximum current, both the reversible displacement and the current decrease with decreasing field. This correlation indicates a softening of the vortex lattice and a shear limited current.

ACKNOWLEDGMENTS

The authors would like to thank A. Will for technical assistance. This work was partly supported by the Bundesministerium für Forschung und Technolgie under Grant No. 13N6177.

[1]E. J. Kramer, J. Appl. Phys. **44**, 1360 (1973).
[2]S. J. Mullock and J. E. Evetts, J. Appl. Phys. **57**, 2588 (1985).
[3]D. Dew-Hughes, Philos. Mag. B **55**, 459 (1987).
[4]H. Küpfer and T. Matsushita, J. Appl. Phys. **63**, 5060 (1988).
[5]A. M. Campbell, J. Phys. C **2**, 1492 (1969).
[6]A. M. Campbell, J. Phys. C **2**, 3186 (1971).
[7]R. Doyle A. M. Campbell, and R. E. Somekh, Phys. Rev. Lett. **71**, 4241 (1993).
[8]H. Küpfer and A. A. Manuel, Phys. Status Solidi A **54**, 153 (1979).
[9]A. M. Campbell *et al.*, *Proceedings of the International Symposium on Flux Pinning and Electromagnetic Properties of Superconductivity, Fukuoka, Japan, 1985,* edited by T. Matsushita, K. Yamafuji, and F. Irie (Matsukama, Fukuoka, Japan, 1985), p. 54.
[10]T. Matsushita and H. Küpfer, J. Appl. Phys. **63**, 5048 (1988).
[11]R. W. Rollins *et al.*, J. Appl. Phys. **45**, 5932 (1974).
[12]H. R. Kerchner, J. Low Temp. Phys. **34**, 33 (1978).
[13]P. W. Anderson and Y. B. Kim, Rev. Mod. Phys. **36**, 39 (1964).
[14]A. Gurevich *et al.*, Phys. Rev. B **44**, 12 090 (1991).
[15]A. Gurevich and H. Küpfer, Phys. Rev. B **48**, 6477 (1993).
[16]S. N. Gordeev *et al.*, Phys. Rev. B **49**, 15 420 (1994).
[17]R. Kresse *et al.*, *Proceedings of the First European Conference on Applied Superconductivity,* Applied Superconductivity, edited by H. C. Freyhardt (DGM Informationsgesellschaft, Oberosel, 1993), Vol. 1, p. 337.
[18]T. Matsushita *et al.*, Jpn. J. Appl. Phys. **28**, 356 (1989).
[19]T. Matsushita *et al.*, Cryogenics **33**, 347 (1993).
[20]R. Meier-Hirmer *et al.*, Phys. Rev. B **31**, 183 (1985).
[21]H. Küpfer *et al.*, Adv. Cryogenic Eng. Mater. **34**, 725 (1988).
[22]R. Wördenweber, Phys. Rev. B **46**, 3076 (1992).
[23]K. Kimura *et al.* (unpublished).
[24]A. A. Zhukov *et al.*, Phys. Rev. B **51**, 12 704 (1995).
[25]I. Maksimov *et al.* (unpublished).
[26]A. A. Zhukov *et al.*, Physica C **235-240**, 2837 (1994).
[27]C. Keller *et al.*, Cryogenics **30**, 401 (1990).
[28]E. J. Tomlinsen *et al.*, Cryogenics **33**, 28 (1993).
[29]R. A. Doyle *et al.*, *Proceedings of the First European Conference on Applied Superconductivity,* Applied Superconductivity (Ref. 17), p. 689.
[30]A. I. Larkin and Yu. N. Ovchinnikov, J. Low Temp. Phys. **34**, 409 (1979).
[31]G. Blatter *et al.*, Rev. Mod. Phys. **66**, 1125 (1994).
[32]H. Küpfer *et al.*, Phys. Rev. B **50**, 7016 (1994).